Université Paris Diderot - Paris 7

Politecnico di Torino

M2 Quantum Devices

Internship Report

Bipolar transistor for pH biosensors

IBM T.J. Watson Research Center, Yorktown Heights, NY

Author:
Giulia Prone

Supervisor:
Sufi Zafar

Manager:
Luisa Bozano

June 15, 2018

To my parents. Without them, I wouldn't be who I am.

To my boyfriend, Jessy, who supported me every day.

Acknowledgement

First, I would like to thank Dr. Sufi Zafar, research member at IBM T.J. Watson Research Center, who accepted me for this internship and always managed to be available in spite of her enormous volume of work. She helped me not only in carrying out the experiments, but also in writing my report and preparing my presentation.

My thanks goes to Luisa Bozano, manager of Nanoscale Fabrication Group at IBM Almaden Research Center, who together with Dr. Zafar gave me this opportunity and helped me with all the official work with great patience.

A lot of thanks goes to Dr. Maria Luisa Della Rocca, who followed, supported, and helped me and my colleagues during our master's degree, during the choice and the associated paperwork of our internships.

Sara, Aldo, Carlo, Giacomo and Claudia are also thanked for their presence which made the lab and the workplace such a pleasant place to be. Finally, a really big thanks to my friend and colleague Salvo for listening to my queries, offering me advice, and supporting me through these years.

The Thomas J. Watson Research Center serves as the headquarters of IBM Research, one of the largest industrial research organizations in the world. Scientists at T.J. Watson are pioneering scientific breakthroughs across today's most promising and disruptive technologies including the future of artificial intelligence, blockchain and quantum computing.

My team is split between the IBM Research Center in Yorktown Heights and the IBM Research Center in San Jose California. I work in the first one. This team deals with Materials for Advanced Technology, Nanoscale Fabrication and Sensors.

Abstract

A sensor is a transducer that receives and responds to a signal or stimulus from a physical system. It produces a signal representing information about the system, which is used by some type of telemetry, information or control system.

Specifically, a biosensor is a device that contains a biological, or bio-inspired recognition layer with unique specificity towards target analytes, which can be pH, DNA, proteins, and small molecules like glucose, chemical warfare agents or environmental pollutants. The focus on electrochemical sensors and biosensors is growing exponentially, as these detection systems can be easily miniaturized and mass-produced for point-of-care applications.

Electrochemical sensors are significantly impacted from the choice of the transducers characteristics. Field effect transistors (FET) have been widely used as transducers in electrochemical sensors for over 40 years. However, a completely new discovery has been made in this field, using a bipolar junction transistor (BJT) as transducer instead of a Field Effect Transistor (FET).

The goal of this work is to use this type of device for the analysis of different analytes, in particular alcohol and sodium chloride solutions.

Particularly in this internship, the sensor will be added to an array of sensors to be placed inside the artificial nose which is being developed at IBM's headquarters in Almaden.

Index

List of Figures

Chapter 1

Introduction

1.1 State of the Art

Over the past decade, sensors based on silicon field effect transistors (FETs) have emerged as the main class of sensors due to their enhanced sensitivity and fabrication compatibility with silicon processing technology [1, 2]; but also for their enhanced sensitivity, resolution, low power, and portability. Moreover, these electrochemical sensors have been demonstrated to detect both ions and biomolecules [3, 4].

The application of FETs as transducers in electrochemical sensors was first described in 1970 by Bergveld [5]. Triggered by this discovery, FET based electrochemical sensors have been extensively investigated. Due to their small size, the nanowire FET sensors offer two important advantages: fast response time and high sensitivity due to large surface-to-volume ratios [6]. Several studies have investigated pH sensing using silicon nanowire FET sensors [7, 8].

In particular, the pH value plays a critical role in numerous biochemical reactions and is of maximum importance in the study of life sciences [9, 10]. For example, the activity of proteins [11], enzymes [8], cellular organelles [12] and cells [13] are drastically affected by minute changes in pH value. Also, the pharmacological effectiveness of drugs can be altered by changing the pH of their local environment [14]. Hence, the ability to monitor pH with high sensitivity and spatial resolution can help clarify many physiological processes with applications in drug discovery and medical diagnostics [6]. Also, pH sensing plays an important role in environmental and food industry related applications [15]. Hence, accurate and fast sensing of pH is of great interest in various fields of study.

Sensors based on silicon field effect transistors exhibit pH-dependent conductance that is linear over a large dynamic range and could be understood in terms of the change in surface charge during protonation and deprotonation [7, 16]. However, their practical applications have been hindered due to significant sensor-to-sensor variations in the detection characteristics and these features also vary in a complex manner over the entire sensing field [17]. Thus, detailed calibrations for individual sensors must be performed before these nanowires can be used reliably for sensing quantities.

Recently, bipolar junction transistor (BJT) device was proposed as a transducer in an electrochemical sensor [18, 19, 20]. BJT pH biosensors have been created the first time in 2015 by Dr. Sufi Zafar, my mentor and supervisor in this project.

For the BJT sensor, a signal to noise ratio of 20 to 2 times greater has been found. Sensitivity is also enhanced, changing by 10 times per part for the BJT sensing signal. However, the FET signal changes by at most 8 times in a complex manner over the sensing range and exhibits significant variations from sensor to sensor induced by the fabrication process. Also, sensor calibration curves (a method for determining the concentration of a substance in an unknown sample by comparing it to a set of standard samples of known concentration) are impacted by the transducer choice in case of FET sensor. However, the calibration curve of a BJT sensor is independent of applied voltages. Furthermore, the bipolar transistor Signal-to-Noise Ratio (SNR) is not only significantly higher but is also constant over the sensing range. In comparison, the SNR of a FET sensor varies with the peak value confined within a narrow sensing range [21].

Biosensors based on bipolar transistors are shown to have superior sensory characteristics that require minimal calibrations – an important characteristic for mobile sensing applications. They are also significantly better suited for quantitative sensing measurements and detection applications.

The aim of this work is to characterize the BJT biosensor designed by Dr. Zafar for different analytes. This is the first step that will allow for the application of this innovative device for the detection of alcohol and sodium chloride substances. This kind of sensor has also been applied for single strand DNA detection [22] and mobile diagnostic applications [23].

1.2 Theory

1.2.1 Electrochemical sensor

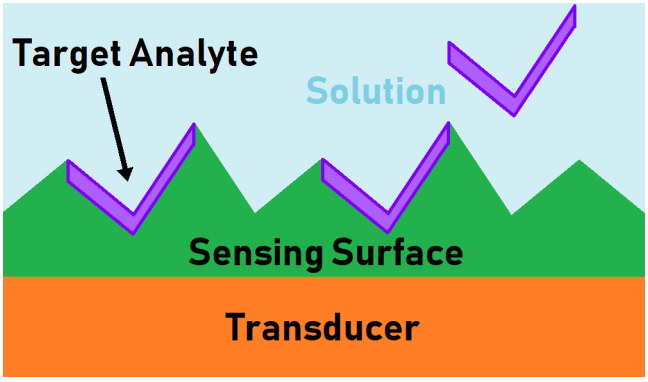

Figure 1.1: Schematic electrochemical sensor. The sensor components are the sensing surface and the transducer; the sensing surface is in contact both with the solution and the dissolved target analyte, that selectively bind to the sensing surface.

An electrochemical sensor has two basic components (Fig. 1.1):

- the sensing surface (or receptor)
- the transducer

The sensing surface interacts with the target analyte and the transducer converts this interaction into a readable electronic signal. The sensor performance characteristics depend on both the components. The sensor selectivity and affinity towards the target analyte depends solely on the sensing surface because the analyte interacts only at the sensing surface, as illustrated in Figure 1.1. Other performance metrics such as sensitivity, resolution, and calibration depend on both components.

In this project, the electrochemical sensor with bipolar junction transistor (BJT) will be used as the transducer. This because SNR, sensitivity and calibration curves are independent of measurement voltages for the BJT sensor [23]. This implies that optimal measurements can be made over the entire sensing range with minimal calibration requirements.

1.3 Bipolar Junction Transistor

A bipolar junction transistor consists of two back-to-back p-n junctions, which share a thin common region. Contacts exist between either of the two outer regions (called the emitter and collector) and the middle region (called the base). The device is called "bipolar" since its operation involves both types of mobile carriers, viz. electrons and holes.

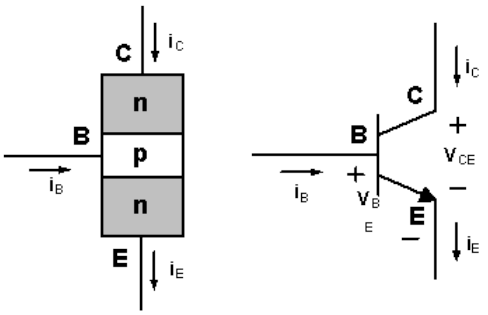

Figure 1.2: Schematic NPN BJT device.

There are four different bias modes: the forward active mode of operation, the reverse active mode of operation, the saturation mode and the cut-off mode.

In this kind of application, the forward active mode of operation will be used. This is obtained by forward-biasing the base-emitter junction and, in addition, eliminating the base-collector junction current by setting $V_{BC} = 0$.

1.4 Experimental Setup

The biosensor has two components:

- the device, and
- an extended base.

The device component is the commercial 2N2222A, which is a common NPN bipolar junction transistor (BJT) used for general purpose low-power amplifying or switching applications. It is designed for low to medium current (up to $500mA$), low power and medium voltage. This is the desired range of work in order to avoid any kind of chemical reaction between the tip sensing surface and the reference electrode with the aqueous solutions.

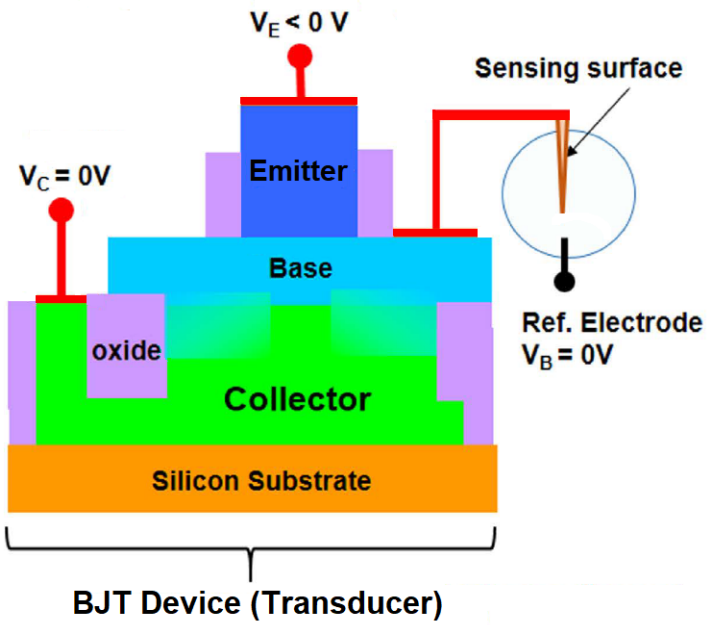

Figure 1.3: Schematic of an electrochemical sensor with a BJT device as the transducer [23].

As shown in Figure 1.3, the extended base component consists of:

- a conducting sensing surface connected to the base at one end, while the other end is immersed in the aqueous solution;
- a miniaturized reference electrode immersed in the aqueous solution.

The sensing surface is a $100nm$ thick TiN film sputter deposited over a tungsten (W) wire. The pH sensing surface for the BJT biosensor will be made of titanium nitride material since the TiN surface potential is pH sensitive [24].

Here, the voltages applied at the emitter, collector and reference electrode are V_E, V_C and V_B respectively. The collector current (I_C) is the sensing signal and sensing measurements are made using $V_C = V_B = 0V$, while V_E is either varied or set at a fixed value.

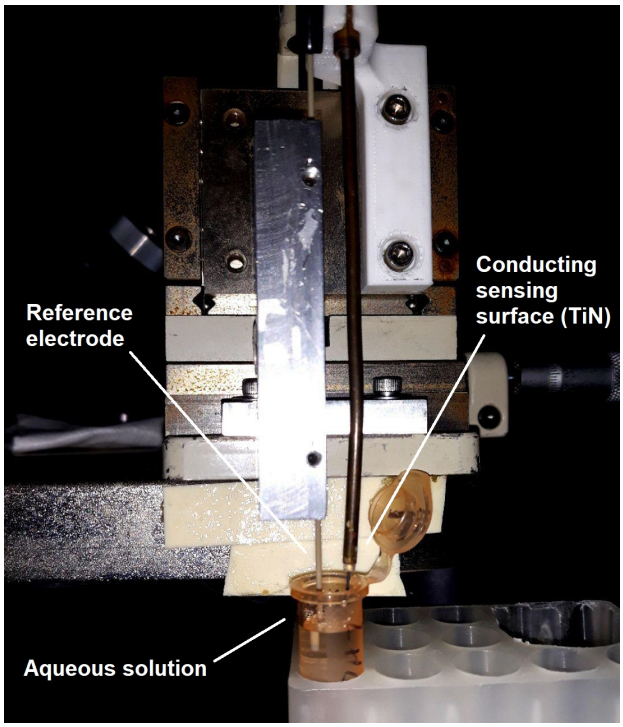

Figure 1.4: Real image of the extended base set-up of the BJT electrochemical sensor.

1.5 Physical description

Like the standard bipolar transistor, the transfer curve of the bipolar transistor biosensor in active mode is given by the Ebers-Moll equation [25]. It has been modified by [21] in order to synchronize with the physical model, evolving the following equation for the sensing signal I_C:

$$I_C = I_0 \cdot e^{q \cdot (V_{BE} + \psi_S)/kT} \tag{1.1}$$

where, T is the temperature in Kelvin, k is the Boltzmann constant, I_0 is a BJT device constant, q is the electronic charge and $V_{BE} = (V_B - V_E)$. Moreover, the sensing surface potential ψ_S depends solely on the sensing surface charge density associated with the bound analyte, and is therefore a characteristic of the sensing surface/analyte interaction. This interaction represents the core of the sensing process.

From Eq. (1.1), it is clear that I_C depends exponentially on the surface potential ψ_S of the sensing film. Also, since ψ_S depends on the surface charge density, a change in charge density associated with bound ions or molecules within the Debye length would cause the sensing current I_C to vary, which can be easily detected. The Debye length is the spatial distance within which the mobile electric charges screen the electric field.

1.6 Equipment

Figure 1.5: B1500A Semiconductor Device Parameter Analyzer (left). Equipment used to analyze the BJT biosensor (right).

For all the experiments, the used equipment setup is the B1500A Semiconductor Device Parameter Analyzer and Measurement Modules (Figure 1.5 (left)) [26]. This is a semiconductors device precision current-voltage analyzer, and it is an all-in-one analyzer supporting I/V, C/V, pulse/dynamic I/V, and many others measurements. It provides a wide range of measurement capabilities to cover the electrical characterization and evaluation of devices, materials, semiconductors, active/passive components (or virtually any other type of electronic device) with uncompromised measurement reliability and efficiency.

During the performance of all the measurements, a compliance of $1\mu A$ is maintained in order to avoid damage to the used BJT. As shown in Figure 1.5 (right), the BJT biosensor is linked to the equipment via PIN connections, where PIN 1 and PIN 3 are connected to the emitter and collector respectively, while PIN 2 is connected to the extended base described previously (see section 1.3).

1.7 Objectives and problem to solve

The entire study has been performed in order to be part of a larger project conducted in IBM Research-Almaden (San Jose, California) concerning the idealization and implementation of an artificial nose. Specifically, this sensor will be part of the array of sensors to be placed inside the device.

The main goal of my work is to find the sensor response to different types of solutions. Specifically, sodium chloride ($NaCl$) and alcohol (C_2H_5OH) solutions at different concentrations will be analyzed. In order to do this, the sensing surface has to be characterized. This is done creating the calibration curve using pH buffer solutions having a known pH value. Here, the voltage / pH curve at constant current will help in finding the pH of different solutions. This is explained in more detail in the following chapter (see section 2.1).

During this kind of measurements, errors can occur from several sources:

- drift,
- electrochemical reactions, or
- evaporation of the solutions (especially alcohol).

In the following, these problems will be minimized by optimizing the experimental setup and looking for solutions for storage of the analytes.

Chapter 2

Measurements and Results

In this chapter, the analysis of Alcohol and sodium chloride solutions will be carried out through the study of the corresponding pH change. These two analyses are reported in sections 2.2 and 2.3 respectively. In order to do this, the characterization of the tip (to be used in the subsequent analysis) must be performed, which is reported in section 2.1.

2.1 pH buffers

As already mentioned, in order to characterize the tip used in all subsequent experiments, the calibration curve for the TiN sensing surface tip is necessary.

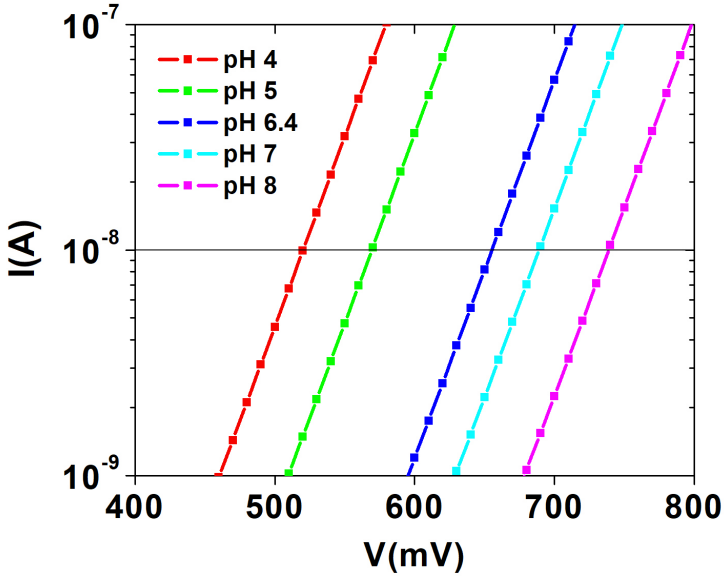

Figure 2.1: I_C dependence on V_{BE} measured at different pH buffer solutions. Here, the measured $SS = 59mV/decade$, irrespective of the pH values.

Hydrion Buffer powders are used to create the buffer solutions, diluting the powders in $500mL$ of deionized water. This is done in order to find the values of the voltages corresponding to each pH, keeping the current fixed. Subsequently, the resulting calibration curve will be used to derive the pH values of the others analytes, like alcohol and $NaCl$.

Prior to discussing the sensing results for the BJT biosensor in buffer solutions, the measurement details are described. The sensing signal I_C is measured by varying the applied emitter voltage (V_E) in the range of $0V$ to $-0.8V$, while the base voltage (V_B) applied to the reference electrode and the collector voltage (V_C) applied to the collector are set to $0V$.

All sensing measurements are confined to the voltage regime below the onset of the high injection effect, where the I/V characteristic result is linear. The high injection effect is a typical non-linear effect taking place in the forward active operation mode. Overcoming this level, the slope of the curve at high I_C begins to decrease.

The used buffers are solutions of varying pH values: pH8, pH7, pH6.4, pH5, pH4. All measurements are made at room temperature.

First of all, the sensing currents I_C as functions of the applied voltages $V_{BE} = (V_B - V_E)$ are measured. Figure 2.1 shows the dependence of I_C on the applied V_{BE} measured at different pH values of the buffer solution. Circular symbols represent the measurements, while solid lines are exponential fits in accordance with Eq. (1.1). It is important to notice that the measurements indicate I_C increases exponentially with a Subthreshold Swing $SS = 59mV/decade$, irrespective of the pH value. The SS is derived by calculating the difference between the corresponding voltages at $I_C = 3 \cdot 10^{-9}A$ and $I_C = 3 \cdot 10^{-8}A$.

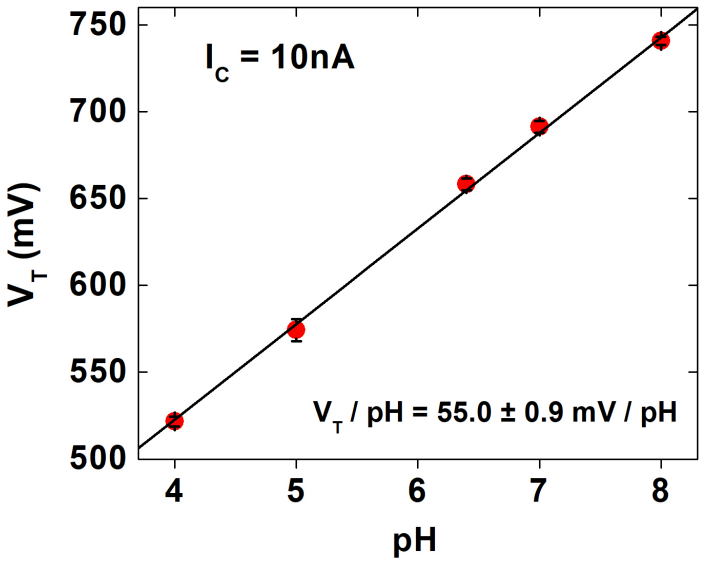

Figure 2.2: V_T dependence on pH derived by 2.1 at $I_C = 10nA$. Here, the measured slope is $55.0 \pm 0.9mV/pH$.

Since the sub-threshold swing (SS) is defined as the change in V_{BE} corresponding to a decade change in I_C, we have $SS = 2.3 \cdot kT/q$. Hence from equation (1.1):

$$I_C = I_0 \cdot e^{2.3 \cdot (V_{BE} + \psi_S)/SS} \tag{2.1}$$

where, $T = (q \cdot SS)/(2.3 \cdot k)$.

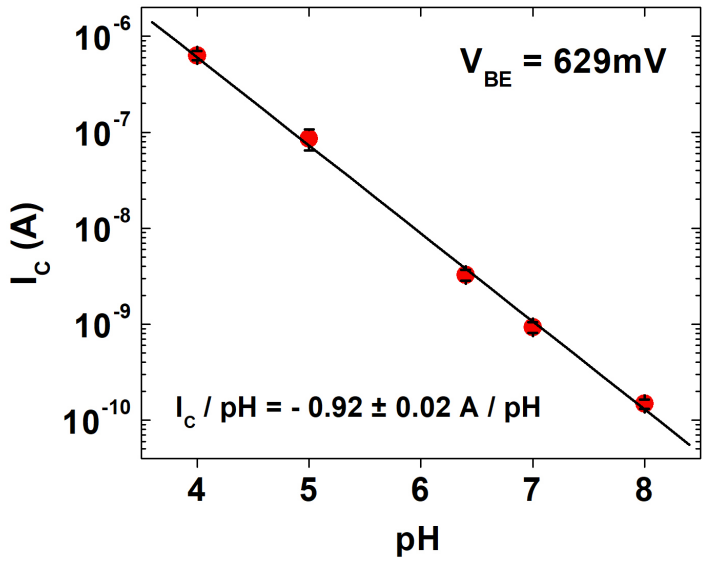

Figure 2.3: I_C dependence on pH derived by 2.1 at $V_{BE} = 629mV$. Here, the measured slope is $0.92 \pm 0.02A/pH$.

With $SS = 59mV/decade$, $q = 1eV$, and $k = 8,61673324 \cdot 10^{-5}eV \cdot K^{-1}$, the estimated temperature is $T = 297.7K = 24.6$°C from the measured SS, consistent with the room temperature value. Hence, the measured transfer curves are in quantitative agreement with Eq. (2.1). Also, the measured I_C curves are observed to shift by $55mV/pH$ as the pH is varied. This is a property of the TiN sensing surface.

From Figure 2.1 it is now possible to derive the calibration curve, which characterizes each reference tip, and is unique for each type of tip even if the materials are the same. In fact it also depends on the type and the conditions of the deposition.

V_T is defined as the applied voltage value corresponding to a constant sensing current of $I_C = 10nA$.

In the Figure 2.2 the calibration curve has been created repeating the measurements of the buffer solutions 9 times, both randomly and in an ordered way. Between two measurements, the reference-tip setup has been rinsed with deionized water in order to remove any kind of dependence from the previous measurement. The vertical black error bar represents the standard deviation, which has been calculated with the aid of the OriginLab statistical software, while horizontally the error present in the pH powder for the creation of the solutions is estimated as ± 0.02.

Figure 2.3 represents a different type of calibration curve. This is created by fixing the voltage value and considering the current shift at different pH values. The chosen fixed voltage is $V_{BE} = 629mV$, since at this value all the curves become linear in the range in which they are used. Here the measured curves are observed to shift by $-0.92A/pH$ (in logarithmic scale) as the pH is varied.

Both of these calibration curves (Figures 2.2, 2.3) will be used in the following sections to analyze the pH values of the studied analytes.

In order to obtain small voltage errors during the repetition of the measurements, and then a small drift, the tip-reference setup has been rinsed as mentioned previously. Furthermore, the tip-to-reference distance, as well as the amounts of tip and reference that were immersed, have been kept constant during all the measurements.

2.2 pH vs. Alcohol

The analysis conducted with the buffer solutions can now be used to estimate the pH values of alcohol solutions at different concentrations and to implement further analysis.

2.2.1 Solutions creation

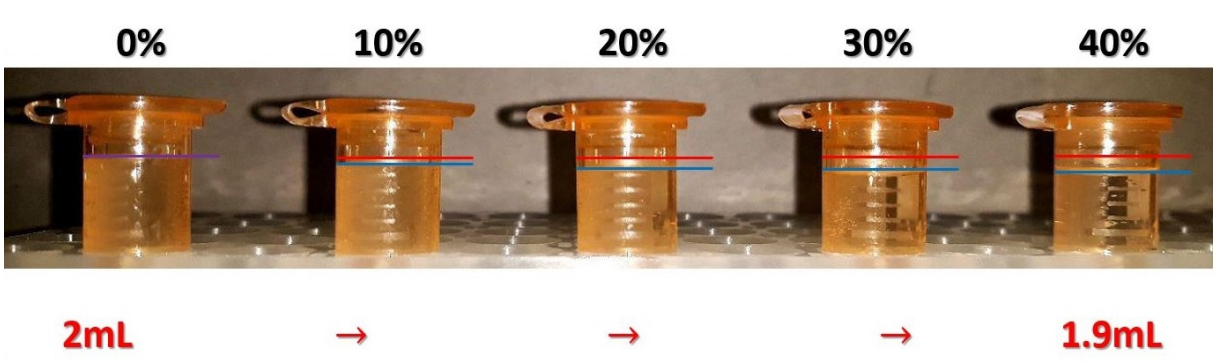

Figure 2.4: Images of the alcohol solutions immediately after their creation. The volume decrease (indicated by a pair of red and blue lines) is directly proportional to the increase in alcohol percentage.

Before beginning the data analysis, it is important to take a look to the reactions which take place during the mixing of alcohol and water.

Here, the analytes are created mixing $1mM$ concentrated $NaCl$ solution with different ethanol (C_2H_5OH) percentage: 0%, 10%, 20%, 30% and 40%. The alcohol used is the Ethyl Alcohol, Reagent Alcohol 200 Proof, PHARMCO-AAPER^{TM}. A sodium chloride solution $[NaCl] = 1mM$ is used instead of deionized water in order to enhance conduction. In fact, for a solution to conduct electricity, presence of free ions is necessary. Hence alcohol, which does not ionize, is a bad conductor of electricity. The electrical conduction is necessary in order to obtain a resistive response from the biosensor.

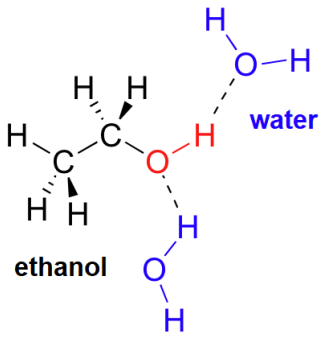

Figure 2.5: Schematic of the ethanol-water Hydrogen bonding.

As shown in Figure 2.4, a decrease in volume from $2mL$ at 0% alcohol concentration to $1.9mL$ at 40% takes place. The physical explanation of this phenomenon [27, 28] is as follows: both water and ethanol have small hydrogen atoms attached to an oxygen atom, which strongly attracts the

shared electron cloud between the two. This makes the hydrogen nucleus (a proton) to be relatively exposed, and given the very small atomic radius of the former, a high moment molecular electric dipole is formed. These dipoles tend to attract each other in different molecules, and the resulting inter-molecular interaction implies that this kind of chemical species pack molecules very closely and bonds them together strongly with hydrogen bond ("H-bond"), as shown in Figure 2.5.

The formation of hydrogen bonds does not limit itself to identical molecules, but they cross-form among different H-bond forming chemical species in a mixture; this is what happens between water and ethanol: the oxygen in one water molecule is attracted to the hydrogen in the hydroxyl group (the red one in the Figure 2.5) in a nearby alcohol molecule and viceversa. The H-bonds pack the molecules together in the liquid phase, which produces the macroscopically observed increase in density and total volume reduction. The strong interaction implies a reduction in the internal energy of the system which manifests as the liberation of energy in the form of heat [29]. This explain the immediate change of volume of around 5% of volume between 0% and 40% alcohol concentration just after the creation of the solutions.

A deeper analysis of the pH dependence of alcohol with respect to time and concentration can now be performed.

2.2.2 pH dependence with time and alcohol concentration

In order to perform this study, first of all measurements of the sensing current I_C as a function of the applied voltage $V_{BE} = (V_B - V_E)$ are performed.

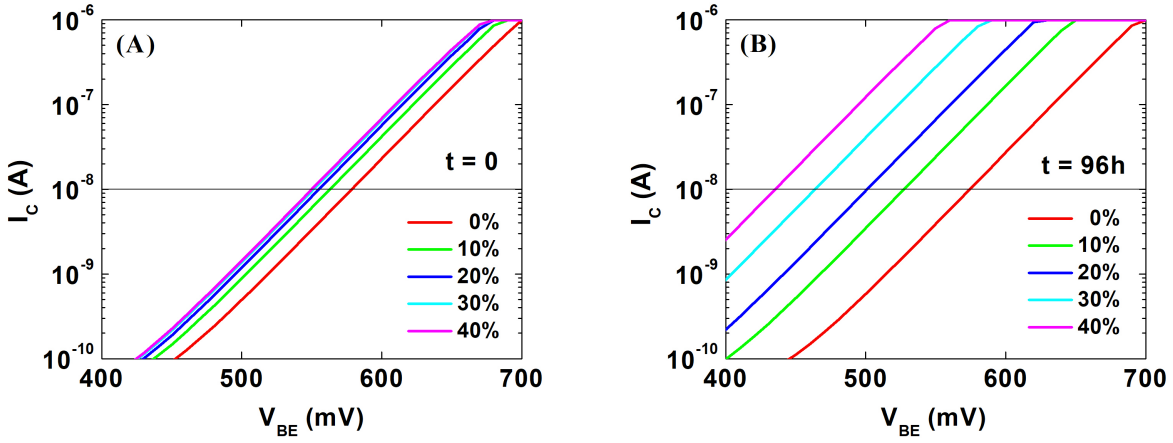

Figure 2.6: I_C dependence on V_{BE} measured at different alcohol concentrations in $[NaCl] = 1mM$ solutions. **(A)** Current/Voltage characteristic at time zero, just after the creation and the mixing of the solution. **(B)** Current/Voltage characteristic after 96h. The solutions are conserved at 4°C, in order to avoid evaporation.

Figures 2.6 (A) and (B) show the dependence of I_C on the applied V_{BE} measured at different alcohol concentrations. Here, all the curves show the same slope independent of the alcohol concentration.

The characteristics have been measured just after the creation and the mixing of the solutions (Figure 2.6 (A)) and after 4 days (Figure 2.6 (B)). In order to avoid possible evaporation, all the solutions were conserved at 4°C continuously just after the first measurements, and placed at room temperature for one hour before the second measurements were taken – so that all the experiments are performed at the same initial conditions.

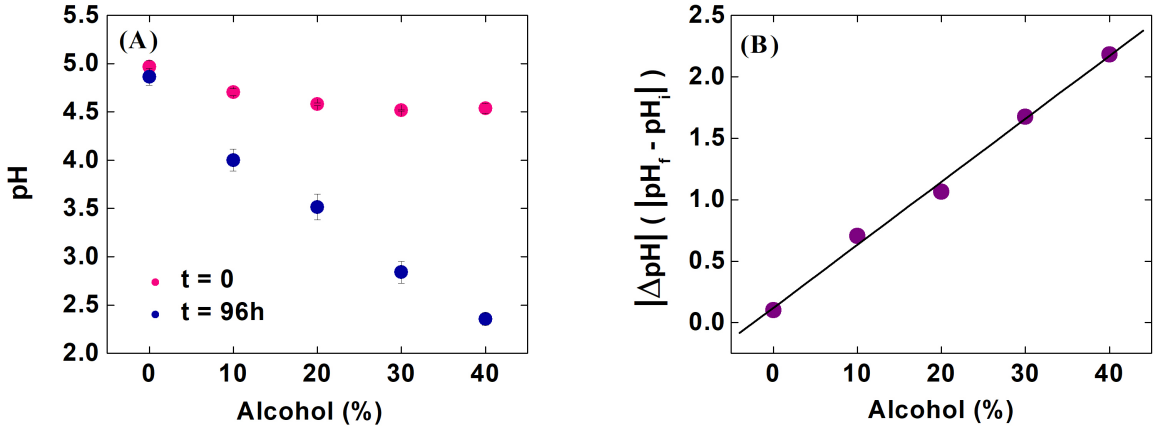

Figure 2.7: pH dependence on Alcohol percentage measured in different time periods, just after the creation of the solutions and after 4 days. The chemicals are $[NaCl] = 1mM$ solutions at different alcohol concentrations. **(A)** pH/Alcohol characteristics at time zero (pink) and after 96h (blue). **(B)** ΔpH/Alcohol characteristic describing the amount of change of pH with respect to the alcohol percentage.

Also in this case, as already seen for buffer solutions and as expected, the measurements show I_C increases exponentially with $SS = 59mV/decade$, irrespective of the alcohol concentration. The SS is derived from the difference between the corresponding voltages at $I_C = 2 \cdot 10^{-9}A$ and $I_C = 2 \cdot 10^{-8}A$. Moreover, the measured I_C curves are observed to shift by different $mV/alcohol(\%)$ as the alcohol concentration is varied. This is probably do to the many complex reactions which take place in alcohol-water solution, as described in literature from a chemical point of view [30].

In order to extrapolate the pH of these solutions, the V_{BE} values at $I_C = 10nA$ are compared with the calibration curve which has been previously obtained in Figure 2.2. From Figure 2.7 (A) it is possible to see that, just after the creation, the pH values result to be almost constant and around 4.8 ± 0.2 with a slightly increase of acidity with the increasing of alcohol concentration, while after 96 hours the diminution of pH with respect to alcohol percentage is more pronounced, reaching a pH of 2.3. This general behavior of decreasing pH values with increasing alcohol concentration can be explained looking to the reaction occurring between ethanol and alcohol [32]:

$$C_2H_5OH + H_2O \iff C_2H_5O^- + H_3O^+$$

As shown in the reaction, the creation of hydrogen ions increases the density of H^+ ions bounded to the sensing surface, thereby causing surface potential ψ_s to shift with a concomitant shift in V_T: i.e. $\Delta V_T = \Delta\psi_s$. It is therefore clear that on increasing the alcohol concentration the acidity of the solution will increase.

The exact cause for the difference in behavior observed at time zero and after 96 hours could not be clearly understood. However this could be possibly due to two main reasons:

- the alcohol-water mixing might be a slow process, in which case an intimate and complete equilibrium of the two could take some time to achieve;
- the carbon dioxide absorption occurring when the solutions are exposed to air could produce a lowering of the pH values. This because the water used for the creation of the solutions is deionized, and existing literature suggests that exposing deionized water to atmosphere could cause an increase of acidity [31].

From Figure 2.7 (B) it is possible to see how the difference between the final pH values (pH_f) after 4 days and the initial ones (pH_i) at time zero increases with increasing alcohol concentration, following a linear trend with a slope of 0.051 ± 0.002 $\Delta pH/alcohol(\%)$. This graph is just a more explicit representation of the first one (Figure 2.7 (A)) which shows the increase in acidity observed with alcohol, together with the increase in acidity due to the exposition of the entire solution to open atmosphere – where consequent absorption of carbon dioxide is much more pronounced for higher concentrations of alcohol. This can be explained taking into account the two previous hypothetical reasons.

2.2.3 Sensing current noise power density

The analysis of the sensing current noise power density is important in order to provide an estimate of the detection limit.

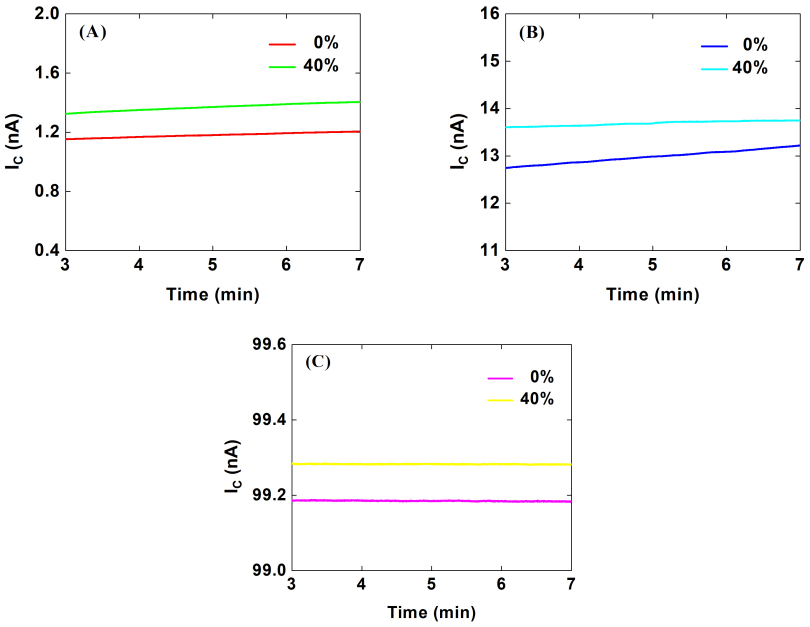

Figure 2.8: Time dependence of 0% and 40% alcohol solutions with respect to time at values around $I_C = 1nA$ **(A)**, $I_C = 10nA$ **(B)**, $I_C = 100nA$ **(C)**,

From literature [21] it is found to be constant over the entire sensing range for a 0% alcohol concentration. Here a comparison between the sensing current (S_I) noise power density for solutions with alcohol and solution without alcohol is performed.

The noise spectral density is the noise power per unit of bandwidth, which is the power spectral density of the noise. In general, the power spectral density (PSD) function shows the strength of the variations (energy) as a function of frequency. In other words, it shows at which frequencies variations are strong and at which frequencies variations are weak. PSD is a very useful tool to find out frequencies and amplitudes of oscillatory signals in time series data, like in this case the noise [33].

The noise power density is defined as the noise power in a bandwidth of $1Hz$, i.e., the noise power per hertz at a point in a noise spectrum. In particular, the sensing current noise power density is an important performance metric for a sensor. Here, the S_I at $1Hz$ is measured for the BJT sensor in alcohol solutions of varying concentrations. The noise measurements are performed, like before, using the Agilent B1500A instrument.

First of all, the collector current I_C is measured as a function of time at a sampling rate of $50ms$ at constant V_E and with $V_C = V_B = 0V$, as shown in Figure 2.8. The measurements are performed at different voltages values in order to obtain a current $I_C = 1nA, 10nA$ and $100nA$ for alcohol concentrations of 0% and 40%.

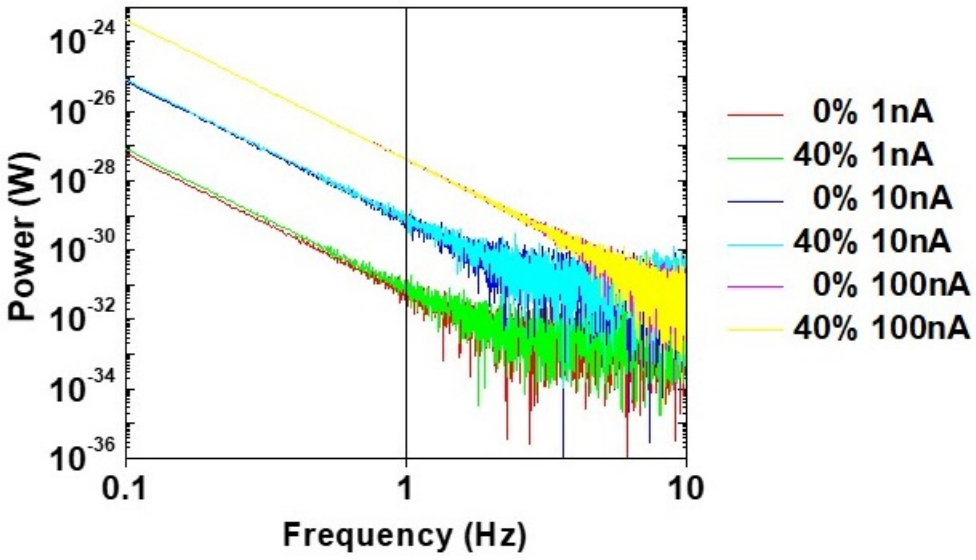

Figure 2.9: Fast Fourier Transform of the current/time data used to extrapolate the the noise power density with respect to the frequency.

The collected time domain data of Figure 2.8 are then analyzed using a Fast Fourier Transform Welch method implemented in Origin software in order to estimate the noise power density (S_I) as a function of frequency. The results are shown in Figure 2.9. It is clear from the obtained plot that the power noise densities are independent of the alcohol concentration.

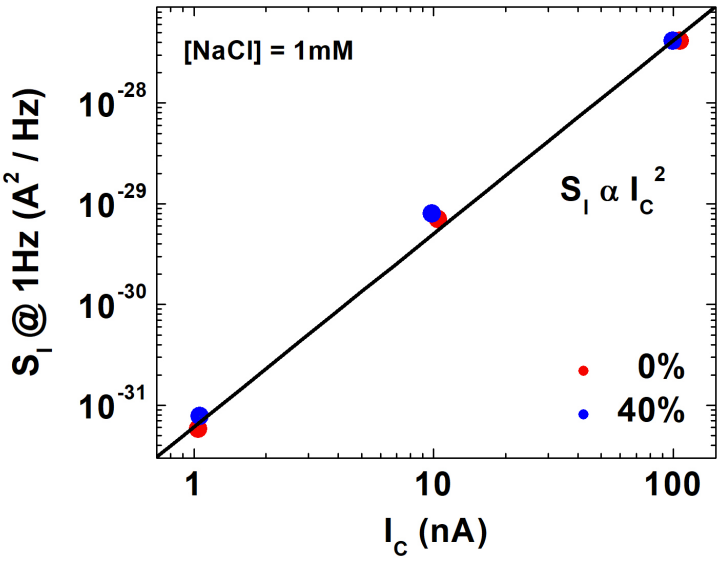

Figure 2.10: Dependence of noise power density (S_I) at $1Hz$ on the sensing current (I_C) measured in solutions of $1mM NaCl$ concentrations at different alcohol percentage.

Figure 2.10 shows the measured dependence of S_I at $1Hz$ on the sensing current I_C for the BJT biosensor. From the graph, it is clear that S_I depends on I_C according to the equation: $S_I = \gamma I_C$, where γ is a constant. Specifically, S_I shows no dependence on the alcohol concentration; and S_I has a power law dependence on the sensing current with an exponent of around 2 (more precisely 1.92 ± 0.09) for BJT sensor. This very much conforms to reports in existing literature [23].

This is definitely a good and encouraging result. As the sensing current noise power density is found to be independent of the presence of alcohol, the low detection limit of a BJT biosensor is not affected by such analytes, and hence its performance remain elevated.

2.3 pH vs. $NaCl$ concentration

A further analysis has been performed in order to calculate the dependence of pH on different sodium chloride concentrations viz.: $1mM, 10mM$ and $100mM$ $[NaCl]$.

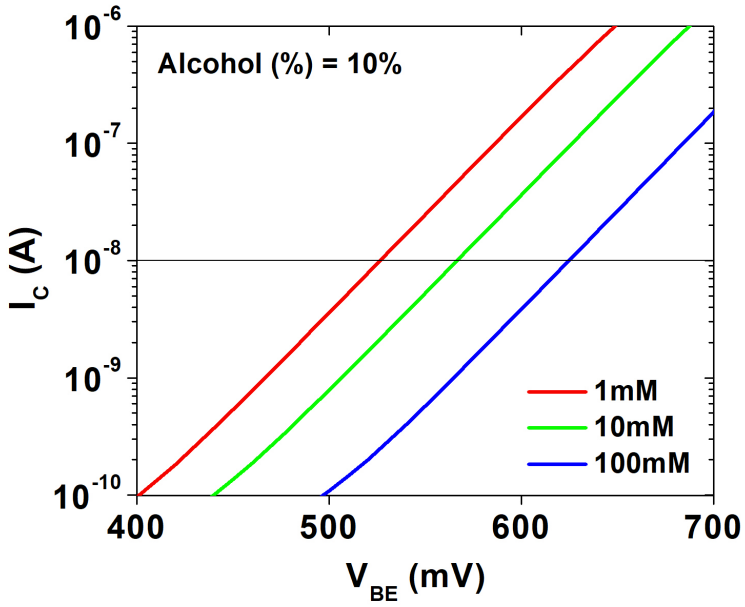

Figure 2.11: I_C dependence on V_{BE} measured at different $NaCl$ concentrations.

The tested solutions have been created by dilution from a $5M$ sodium chloride solution.

Following the previous steps used for the alcohol solutions, measurements of the sensing current I_C as a function of the applied voltage $V_{BE} = (V_B - V_E)$ are performed. Figure 2.11 shows the dependence of I_C on the applied V_{BE} measured at different sodium chloride concentration with a fixed amount of 10% alcohol.

As expected, for different $NaCl$ concentrations also, the measurements show that I_C increases exponentially with $SS = 59mV/decade$, irrespective of the different amounts of sodium chloride present in the solutions. This further observation where SS is found to be independent of the analyzed solutions, leads to the important conclusion that the subthreshold swing (SS) is a property of the BJT biosensor and not of the analytes. The value of SS is derived calculating the difference between the corresponding voltages at $I_C = 2 \cdot 10^{-9}A$ and $I_C = 2 \cdot 10^{-8}A$.

Now, in order to extrapolate the pH of these solutions, the V_{BE} values at $I_C = 10nA$ are compared with the calibration curve previously obtained in Figure 2.2.

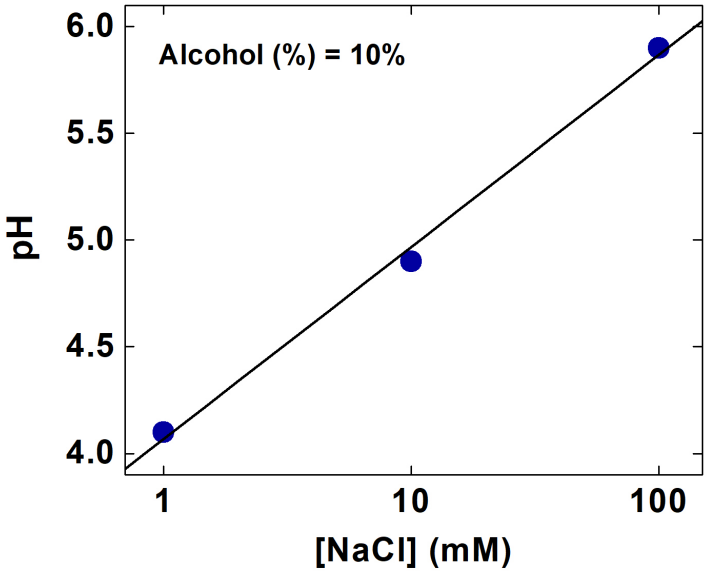

Figure 2.12: pH dependence on sodium chloride ($NaCl$) concentrations. The chemicals are 10% alcohol solutions at different $NaCl$ concentrations.

The obtained pH / $[NaCl]$ dependence is showed in Figure 2.12, where the exponential relation between the sodium chloride concentration and the respective pH is amply clear.

This phenomenon can be easily explained as follows: as chloride concentration increases in the solution, more Cl^- bind to the sensing surface, thereby causing surface potential ψ_s to shift with a concomitant shift in V_T: i.e. $\Delta V_T = \Delta\psi_s$. Here, the observed slope of the characteristic is $0.90 \pm 0.06\ pH/decade$. This result agrees with the phenomena reported in literature [34].

In pure water the pH is expected to be independent of the $NaCl$ concentration, because sodium chloride is a salt formed by a strong acid and a strong base, so it will not undergo hydrolysis. In fact, to observe hydrolysis, at least one of the parent compounds (either the acid or the base or both) should be weak.

On the other hand, with presence of ethanol a dependence of pH on salt concentration is clearly seen, as reported by [34], where, on increasing the $NaCl$ concentration, the solutions show an increase of H_3O^+ ions. Acids components could strengthen the water-ethanol hydrogen-bonding structure and also promote the proton exchange between water and ethanol in $EtOH - H_20$ solutions. With the assistance of the stronger hydrogen-bonding force by acids, ethanol molecules are supposed to be taken into the "water network" to associate with water molecules tightly.

It is then clear that the pH sensor gives a good response also for $NaCl$ solutions.

Conclusion

During this internship, a fully characterization of a pH BJT biosensor based on the previous works of Dr. Sufi Zafar has been realized.

The sensor has been rebuilt and characterized using different buffer pH solutions in order to create the calibration curves at fixed current and voltage values respectively. These curves have been then used to study and analyze the pH values of new analytes: alcohol and sodium chloride ($NaCl$).

Regarding alcohol, a study of the interaction between water and ethanol and its impact on the pH values has been performed giving hypothetical justifications about the behavior of the obtained curves. Alcohol, in fact turned out to be a really difficult and unstable substance due to the many physical reactions occurring, like the mixing with water which produce diminution of volume and heat liberation, the evaporation of alcohol which has been controlled holding the solution at 4°C, the carbon dioxide absorption, etc. Also chemical reactions, as found from literature, affect the stability of the solutions. All these phenomena are reflected in the presence of drift in the I/V curves. Despite all these drawbacks, interesting results have been obtained. An increase of acidity with increasing alcohol concentration has been observed, with a time dependence due to exposition. This could be useful for applications in storage and conservation of beer and wine. Moreover, the sensing current noise power density has been found to be independent of the presence of alcohol. This is a commendable result, as it explains how the low detection limit of this BJT biosensor is not affected by the presence of such analytes, and then its performance remain elevated.

On the other hand, analysis of sodium chloride solutions with constant 10% alcohol show a dependence of pH on salt concentration. Here, the increasing chloride concentration in the solution increases the amount of Cl^- binding to the sensing surface, causing surface potential to shift along with V_T.

Thanks to these results, the integration of this sensor in the artificial nose seems to be possible. Further studies will be conducted by Dr. Sufi Zafar and myself in the next months in order to optimize and better understand the behaviour of these analytes and the response of the sensor with respect to the interaction with them.

Software credit

- Composition: LaTeX
- Data processing: Office Excel 2016 / OriginPro 7.0
- Equipment software: Keysight EasyEXPERT Software

Bibliography

[1] X. P. A. Gao, G. F. Zheng, C. M. Lieber, *Subthreshold regime has the optimal sensitivity for nanowire FET biosensors*, Nano Letters, 10 (2): 547-52, 2010.

[2] E. Stern, J. Klemic, D. Routenberg, P. N. Wyrembak, D. B. Turner-Evans, A. D. Hamilton, D. LaVan, T. M. Fahmy, M. A. Reed, *Label-free immunodetection with CMOS-compatible semiconducting nanowires*, Nature, 445 (7127): 519-22, 2007.

[3] H.-S. Wong, M. H. White, *A CMOS-integrated 'ISFET-operational amplifier' chemical sensor employing differential sensing*, IEEE Trans. Electron Devices 36(3), 479–487, 1989 .

[4] B. R. Dorvel, et al., *Silicon Nanowires with High-k Hafnium Oxide Dielectrics for Sensitive Detection of Small Nucleic Acid Oligomers* ACS Nano 6, 6150–6164 (2012).

[5] P. Bergveld, *Development of an Ion-Sensitive Solid-State Device for Neurophysiological Measurements*, IEEE Trans. Biomed. Eng. 17, 70–71, 1970.

[6] S. Zafar, C. D'Emic, A. Afzali, B. Fletcher, Y Zhu, T. Ning, *Optimization of pH sensing using silicon nanowire field effect transistors with HfO_2 as the sensing surface*, Nanotechnology, 22 (40): 405501, 2011.

[7] Y. Cui, Q. Wei, H. Park, C.M. Lieber, *Nanowire nanosensors for highly sensitive and selective detection of biological and chemical species*, Science, 293: 1289-1292, 2001.

[8] Y. Chen, X. Wang, M. Hong, S. Erramilli, P. Mohanty, *Surface-modified silicon nano-channel for urea sensing*, Sensors and Actuators B: Chemical, 133 (2): 593-598, 2008.

[9] A.S. Yang, B. Honig, *On the pH Dependence of Protein Stability*, Journal of Molecular Biology, 231 (2): 459-474, 1993.

[10] B. Chance, *Effect of pH upon the reaction kinetics of the enzyme-substrate compounds of catalase*, Journal of Biological Chemistry, 194 (2): 471-81, 1952.

[11] N. Nakamura, S.Tanaka, Y. Teko, K. Mitsui, H. Kanazawa, *Four Na+/H+ exchanger isoforms are distributed to Golgi and post-Golgi compartments and are involved in organelle pH regulation*, Journal of Biological Chemistry, 280 (2): 1561-72, 2004.

[12] F. Kamp, P. Donoso, C. Hidalgo, *Changes in luminal pH caused by calcium release in sarcoplasmic reticulum vesicles*, Biophysical Journal, 74 (1): 290-6, 1998.

[13] P. Lipton *Ischemic cell death in brain neurons*, Physiological Reviews, 79 (4): 1431-568, 1999.

[14] K. Katsura, B. Asplund, A. Ekholm, B. K. Siejo, *Extra- and Intracellular pH in the Brain During Ischaemia, Related to Tissue Lactate Content in Normo- and Hypercapnic rats*, European Journal of Neuroscience, 4 (2): 166, 176, 1992.

[15] A. Lubbert, R. Simutis, *Using measurement data in bioprocess modelling and control*, Trends in Biotechnology, 12 (8): 304-311, 1994.

[16] D. Zhang, X. Gao, S. Chen, H. Norstrom, U. Smith, P. Solomon, S.-L. Zhang, and Z. Zhang, *An ion-gated bipolar amplifier for ion sensing with enhanced signal and improved noise performance*, Applied Physics Letters, 105: 082102, 2014.

[17] A. Vacic, M. A. Reed, *Quantitative nanoscale field effect sensors*, Journal of Experimental Nanoscience, 9 (1): 2014, 2013.

[18] P. Das, S. Zafar, *Mechanistic Influence of Nanometer Length-Scale Surface Chemistry on DNA Hybridization*, ACS Nano 9, 7466 –7478, 2015.

[19] J. Cai, T. Ning, J.-B. Yau, S. Zafar, inventors; Globalfoundries Inc. assignee, *Charge sensors using inverted lateral bipolar junction transistors* United States US. 9170338. Oct 27, 2015.

[20] S. Zafar, M. Khattar, V. Jain, T. Ning, *Bipolar junction transistor and nanowire field effect transistor biosensors* Appl. Phys. Lett. 106, 063701, 2015.

[21] S. Zafar, M. Khater, V. Jain, T. Ning, *A comparison between bipolar transistor and nanowire field effect transistor biosensors*, Applied Physics Letters, 106 (6): 063701, 2015.

[22] S. Zafar, T. H. Ning, *Bipolar junction transistor based sensors for chemical and biological sensing*, IEEE Xplore, Solid-State Device Research Conference (ESSDERC), 2016 46th European, 389-392, 2016.

[23] S. Zafar, M. Lu, A. Jagtiani, *Comparison between Field Effect Transistors and Bipolar Junction Transistors as Transducers in Electrochemical Sensors*, Scientific reports, 7: 41430, 2017.

[24] Y. L. Chin, J. C. Chou, Z. C. Lei, T. P. Sun, W. Y. Chung, S. K. Hsiung, *Structures of Anodized Aluminum Oxide Extended-Gate Field-Effect Transistors on pH Sensors*, Japanese Journal of Applied Physics Part 1 40: 6311, 2001.

[25] J. J. Ebers, J. L. Moll, *Large-Signal Behavior of Junction Transistors*, Proceedings of the IRE, 42 (12): 1954.

[26] Origin Data Analysis User Manual (Micorcal Software, Inc., Version 6), pp. 559–563.

[27] G.Onori, A.Santucci, *Dynamical and structural properties of water-alcohol mixtures*, Journal of Molecular Liquids, 69: 161-181, 1996.

[28] F. Franks, D. J. G. Ives, *The structural properties of alcohol-water mixtures*, Quarterly Reviews Chemical Society, 20: 1-44, 1966.

[29] B. Gonzalez, N. Calvar, E. Gomez, A. Dominguez, *Density, dynamic viscosity, and derived properties of binary mixtures of methanol or ethanol with water, ethyl acetate, and methyl acetate at T = (293.15, 298.15, and 303.15) K*, The Journal of Chemical Thermodynamics, 39 (12): 1578-1588, 2007.

[30] R. G. Bates, M. Paabo, R. A. Robinson, *Interpretation of pH measurements in alcohol-water solvents*, Journal of Physical Chemistry, 67 (9):1833–1838, 1963.

[31] B. AJ Reddi, *Why Is Saline So Acidic*, Internationa Journal of Medical Sciences, 10(6): 747–750, 2013.

[32] H. Takahashi, S. Hisaoka, T. Nitta, *Ethanol oxidation reactions catalyzed by water molecules:* $CH_3CH_2OH + nH_2O \leftrightarrow CH_3CHO + H_2 + nH_2O (n = 0, 1, 2)$, Chemical Physics Letters, 363: 80–86, 2002.

[33] P. Stoica, R. Moses *Spectral Analysis of Signals*, Prentice Hall, Inc., 4-12, 2005.

[34] A. Nose, M, Hojo, *Interaction between water and ethanol via hydrogen bonding in alcoholic beverages*, Nova Science Publishers, Inc., 37-91, 2009.